Partial wave analysis of $J/\psi \to \gamma\eta'\eta'$

M. Ablikim,[1] M. N. Achasov,[10,b] P. Adlarson,[68] S. Ahmed,[14] M. Albrecht,[4] R. Aliberti,[28] A. Amoroso,[67a,67c] M. R. An,[32] Q. An,[64,50] X. H. Bai,[58] Y. Bai,[49] O. Bakina,[29] R. Baldini Ferroli,[23a] I. Balossino,[24a] Y. Ban,[39,h] K. Begzsuren,[26] N. Berger,[28] M. Bertani,[23a] D. Bettoni,[24a] F. Bianchi,[67a,67c] J. Bloms,[61] A. Bortone,[67a,67c] I. Boyko,[29] R. A. Briere,[5] H. Cai,[69] X. Cai,[1,50] A. Calcaterra,[23a] G. F. Cao,[1,55] N. Cao,[1,55] S. A. Cetin,[54a] J. F. Chang,[1,50] W. L. Chang,[1,55] G. Chelkov,[29,a] D. Y. Chen,[6] G. Chen,[1] H. S. Chen,[1,55] M. L. Chen,[1,50] S. J. Chen,[35] X. R. Chen,[25] Y. B. Chen,[1,50] Z. J. Chen,[20,i] W. S. Cheng,[67c] G. Cibinetto,[24a] F. Cossio,[67c] X. F. Cui,[36] H. L. Dai,[1,50] J. P. Dai,[71] X. C. Dai,[1,55] A. Dbeyssi,[14] R. E. de Boer,[4] D. Dedovich,[29] Z. Y. Deng,[1] A. Denig,[28] I. Denysenko,[29] M. Destefanis,[67a,67c] F. De Mori,[67a,67c] Y. Ding,[33] C. Dong,[36] J. Dong,[1,50] L. Y. Dong,[1,55] M. Y. Dong,[1,50,55] X. Dong,[69] S. X. Du,[73] P. Egorov,[29,a] Y. L. Fan,[69] J. Fang,[1,50] S. S. Fang,[1,55] Y. Fang,[1] R. Farinelli,[24a] L. Fava,[67b,67c] F. Feldbauer,[4] G. Felici,[23a] C. Q. Feng,[64,50] J. H. Feng,[51] M. Fritsch,[4] C. D. Fu,[1] Y. Gao,[64,50] Y. Gao,[39,h] Y. G. Gao,[6] I. Garzia,[24a,24b] P. T. Ge,[69] C. Geng,[51] E. M. Gersabeck,[59] A. Gilman,[62] K. Goetzen,[11] L. Gong,[33] W. X. Gong,[1,50] W. Gradl,[28] M. Greco,[67a,67c] L. M. Gu,[35] M. H. Gu,[1,50] C. Y. Guan,[1,55] A. Q. Guo,[25] A. Q. Guo,[22] L. B. Guo,[34] R. P. Guo,[41] Y. P. Guo,[9,f] A. Guskov,[29,a] T. T. Han,[42] W. Y. Han,[32] X. Q. Hao,[15] F. A. Harris,[57] K. K. He,[47] K. L. He,[1,55] F. H. Heinsius,[4] C. H. Heinz,[28] Y. K. Heng,[1,50,55] C. Herold,[52] M. Himmelreich,[11,d] T. Holtmann,[4] G. Y. Hou,[1,55] Y. R. Hou,[55] Z. L. Hou,[1] H. M. Hu,[1,55] J. F. Hu,[48,j] T. Hu,[1,50,55] Y. Hu,[1] G. S. Huang,[64,50] L. Q. Huang,[65] X. T. Huang,[42] Y. P. Huang,[1] Z. Huang,[39,h] T. Hussain,[66] N. Hüsken,[22,28] W. Ikegami Andersson,[68] W. Imoehl,[22] M. Irshad,[64,50] S. Jaeger,[4] S. Janchiv,[26] Q. Ji,[1] Q. P. Ji,[15] X. B. Ji,[1,55] X. L. Ji,[1,50] Y. Y. Ji,[42] H. B. Jiang,[42] X. S. Jiang,[1,50,55] J. B. Jiao,[42] Z. Jiao,[18] S. Jin,[35] Y. Jin,[58] M. Q. Jing,[1,55] T. Johansson,[68] N. Kalantar-Nayestanaki,[56] X. S. Kang,[33] R. Kappert,[56] M. Kavatsyuk,[56] B. C. Ke,[44,1] I. K. Keshk,[4] A. Khoukaz,[61] P. Kiese,[28] R. Kiuchi,[1] R. Kliemt,[11] L. Koch,[30] O. B. Kolcu,[54a] B. Kopf,[4] M. Kuemmel,[4] M. Kuessner,[4] A. Kupsc,[37,68] M. G. Kurth,[1,55] W. Kühn,[30] J. J. Lane,[59] J. S. Lange,[30] P. Larin,[14] A. Lavania,[21] L. Lavezzi,[67a,67c] Z. H. Lei,[64,50] H. Leithoff,[28] M. Lellmann,[28] T. Lenz,[28] C. Li,[40] C. H. Li,[32] Cheng Li,[64,50] D. M. Li,[73] F. Li,[1,50] G. Li,[1] H. Li,[64,50] H. Li,[44] H. B. Li,[1,55] H. J. Li,[15] H. N. Li,[48,j] J. L. Li,[42] J. Q. Li,[4] J. S. Li,[51] Ke Li,[1] L. K. Li,[1] Lei Li,[3] P. R. Li,[31,k,l] S. Y. Li,[53] W. D. Li,[1,55] W. G. Li,[1] X. H. Li,[64,50] X. L. Li,[42] Xiaoyu Li,[1,55] Z. Y. Li,[51] H. Liang,[64,50] H. Liang,[1,55] H. Liang,[27] Y. F. Liang,[46] Y. T. Liang,[25] G. R. Liao,[12] L. Z. Liao,[1,55] J. Libby,[21] A. Limphirat,[52] C. X. Lin,[51] D. X. Lin,[25] T. Lin,[1] B. J. Liu,[1] C. X. Liu,[1] D. Liu,[14,64] F. H. Liu,[45] Fang Liu,[1] Feng Liu,[6] G. M. Liu,[48,j] H. M. Liu,[1,55] Huanhuan Liu,[1] Huihui Liu,[16] J. B. Liu,[64,50] J. L. Liu,[65] J. Y. Liu,[1,55] K. Liu,[1] K. Y. Liu,[33] Ke Liu,[17,m] L. Liu,[64,50] M. H. Liu,[9,f] P. L. Liu,[1] Q. Liu,[55] Q. Liu,[69] S. B. Liu,[64,50] T. Liu,[1,55] T. Liu,[9,f] W. M. Liu,[64,50] X. Liu,[31,k,l] Y. Liu,[31,k,l] Y. B. Liu,[36] Z. A. Liu,[1,50,55] Z. Q. Liu,[42] X. C. Lou,[1,50,55] F. X. Lu,[51] H. J. Lu,[18] J. D. Lu,[1,55] J. G. Lu,[1,50] X. L. Lu,[1] Y. Lu,[1] Y. P. Lu,[1,50] C. L. Luo,[34] M. X. Luo,[72] P. W. Luo,[51] T. Luo,[9,f] X. L. Luo,[1,50] X. R. Lyu,[55] F. C. Ma,[33] H. L. Ma,[1] L. L. Ma,[42] M. M. Ma,[1,55] Q. M. Ma,[1] R. Q. Ma,[1,55] R. T. Ma,[55] X. X. Ma,[1,55] X. Y. Ma,[1,50] F. E. Maas,[14] M. Maggiora,[67a,67c] S. Maldaner,[4] S. Malde,[62] Q. A. Malik,[66] A. Mangoni,[23b] Y. J. Mao,[39,h] Z. P. Mao,[1] S. Marcello,[67a,67c] Z. X. Meng,[58] J. G. Messchendorp,[56] G. Mezzadri,[24a] T. J. Min,[35] R. E. Mitchell,[22] X. H. Mo,[1,50,55] N. Yu. Muchnoi,[10,b] H. Muramatsu,[60] S. Nakhoul,[11,d] Y. Nefedov,[29] F. Nerling,[11,d] I. B. Nikolaev,[10,b] Z. Ning,[1,50] S. Nisar,[8,g] S. L. Olsen,[55] Q. Ouyang,[1,50,55] S. Pacetti,[23b,23c] X. Pan,[9,f] Y. Pan,[59] A. Pathak,[1] A. Pathak,[27] P. Patteri,[23a] M. Pelizaeus,[4] H. P. Peng,[64,50] K. Peters,[11,d] J. Pettersson,[68] J. L. Ping,[34] R. G. Ping,[1,55] S. Plura,[28] S. Pogodin,[29] R. Poling,[60] V. Prasad,[64,50] H. Qi,[64,50] H. R. Qi,[53] M. Qi,[35] T. Y. Qi,[9] S. Qian,[1,50] W. B. Qian,[55] Z. Qian,[51] C. F. Qiao,[55] J. J. Qin,[65] L. Q. Qin,[12] X. P. Qin,[9] X. S. Qin,[42] Z. H. Qin,[1,50] J. F. Qiu,[1] S. Q. Qu,[36] K. H. Rashid,[66] K. Ravindran,[21] C. F. Redmer,[28] A. Rivetti,[67c] V. Rodin,[56] M. Rolo,[67c] G. Rong,[1,55] Ch. Rosner,[14] M. Rump,[61] H. S. Sang,[64] A. Sarantsev,[29,c] Y. Schelhaas,[28] C. Schnier,[4] K. Schoenning,[68] M. Scodeggio,[24a,24b] W. Shan,[19] X. Y. Shan,[64,50] J. F. Shangguan,[47] M. Shao,[64,50] C. P. Shen,[9] H. F. Shen,[1,55] X. Y. Shen,[1,55] H. C. Shi,[64,50] R. S. Shi,[1,55] X. Shi,[1,50] X. D. Shi,[64,50] J. J. Song,[15] J. J. Song,[42] W. M. Song,[27,1] Y. X. Song,[39,h] S. Sosio,[67a,67c] S. Spataro,[67a,67c] F. Stieler,[28] K. X. Su,[69] P. P. Su,[47] F. F. Sui,[42] G. X. Sun,[1] H. K. Sun,[1] J. F. Sun,[15] L. Sun,[69] S. S. Sun,[1,55] T. Sun,[1,55] W. Y. Sun,[27] X. Sun,[20,i] Y. J. Sun,[64,50] Y. Z. Sun,[1] Z. T. Sun,[1] Y. H. Tan,[69] Y. X. Tan,[64,50] C. J. Tang,[46] G. Y. Tang,[1] J. Tang,[51] J. X. Teng,[64,50] V. Thoren,[68] W. H. Tian,[44] Y. T. Tian,[25] I. Uman,[54b] B. Wang,[1] C. W. Wang,[35] D. Y. Wang,[39,h] H. J. Wang,[31,k,l] H. P. Wang,[1,55] K. Wang,[1,50] L. L. Wang,[1] M. Wang,[42] M. Z. Wang,[39,h] Meng Wang,[1,55] S. Wang,[9,f] W. Wang,[51] W. H. Wang,[69] W. P. Wang,[64,50] X. Wang,[39,h] X. F. Wang,[31,k,l] X. L. Wang,[9,f] Y. Wang,[51] Y. D. Wang,[38] Y. F. Wang,[1,50,55] Y. Q. Wang,[1] Y. Y. Wang,[31,k,l] Z. Wang,[1,50] Z. Y. Wang,[1] Ziyi Wang,[55] Zongyuan Wang,[1,55] D. H. Wei,[12] F. Weidner,[61] S. P. Wen,[1] D. J. White,[59] U. Wiedner,[4] G. Wilkinson,[62] M. Wolke,[68] L. Wollenberg,[4] J. F. Wu,[1,55] L. H. Wu,[1] L. J. Wu,[1,55] X. Wu,[9,f] X. H. Wu,[27] Z. Wu,[1,50] L. Xia,[64,50] H. Xiao,[9,f] S. Y. Xiao,[1] Z. J. Xiao,[34] X. H. Xie,[39,h] Y. G. Xie,[1,50] Y. H. Xie,[6] T. Y. Xing,[1,55] C. J. Xu,[51] G. F. Xu,[1] Q. J. Xu,[13] W. Xu,[1,55] X. P. Xu,[47] Y. C. Xu,[55] F. Yan,[9,f] L. Yan,[9,f] W. B. Yan,[64,50] W. C. Yan,[73] H. J. Yang,[43,e] H. X. Yang,[1] L. Yang,[44] S. L. Yang,[55] Y. X. Yang,[12] Yifan Yang,[1,55] Zhi Yang,[25] M. Ye,[1,50] M. H. Ye,[7] J. H. Yin,[1] Z. Y. You,[51] B. X. Yu,[1,50,55] C. X. Yu,[36] G. Yu,[1,55] J. S. Yu,[20,i] T. Yu,[65] C. Z. Yuan,[1,55] L. Yuan,[2] Y. Yuan,[1] Z. Y. Yuan,[51] C. X. Yue,[32]

A. A. Zafar,[66] X. Zeng Zeng,[6] Y. Zeng,[20,i] A. Q. Zhang,[1] B. X. Zhang,[1] Guangyi Zhang,[15] H. Zhang,[64] H. H. Zhang,[51] H. H. Zhang,[27] H. Y. Zhang,[1,50] J. L. Zhang,[70] J. Q. Zhang,[34] J. W. Zhang,[1,50,55] J. Y. Zhang,[1] J. Z. Zhang,[1,55] Jianyu Zhang,[1,55] Jiawei Zhang,[1,55] L. M. Zhang,[53] L. Q. Zhang,[51] Lei Zhang,[35] S. Zhang,[51] S. F. Zhang,[35] Shulei Zhang,[20,i] X. D. Zhang,[38] X. M. Zhang,[1] X. Y. Zhang,[42] Y. Zhang,[62] Y. T. Zhang,[73] Y. H. Zhang,[1,50] Yan Zhang,[64,50] Yao Zhang,[1] Z. Y. Zhang,[69] G. Zhao,[1] J. Zhao,[32] J. Y. Zhao,[1,55] J. Z. Zhao,[1,50] Lei Zhao,[64,50] Ling Zhao,[1] M. G. Zhao,[36] Q. Zhao,[1] S. J. Zhao,[73] Y. B. Zhao,[1,50] Y. X. Zhao,[25] Z. G. Zhao,[64,50] A. Zhemchugov,[29,a] B. Zheng,[65] J. P. Zheng,[1,50] Y. H. Zheng,[55] B. Zhong,[34] C. Zhong,[65] L. P. Zhou,[1,55] Q. Zhou,[1,55] X. Zhou,[69] X. K. Zhou,[55] X. R. Zhou,[64,50] X. Y. Zhou,[32] A. N. Zhu,[1,55] J. Zhu,[36] K. Zhu,[1] K. J. Zhu,[1,50,55] S. H. Zhu,[63] T. J. Zhu,[70] W. J. Zhu,[36] W. J. Zhu,[9,f] Y. C. Zhu,[64,50] Z. A. Zhu,[1,55] B. S. Zou,[1] and J. H. Zou[1]

(BESIII Collaboration)

[1]*Institute of High Energy Physics, Beijing 100049, People's Republic of China*
[2]*Beihang University, Beijing 100191, People's Republic of China*
[3]*Beijing Institute of Petrochemical Technology, Beijing 102617, People's Republic of China*
[4]*Bochum Ruhr-University, D-44780 Bochum, Germany*
[5]*Carnegie Mellon University, Pittsburgh, Pennsylvania 15213, USA*
[6]*Central China Normal University, Wuhan 430079, People's Republic of China*
[7]*China Center of Advanced Science and Technology, Beijing 100190, People's Republic of China*
[8]*COMSATS University Islamabad, Lahore Campus, Defence Road, Off Raiwind Road, 54000 Lahore, Pakistan*
[9]*Fudan University, Shanghai 200443, People's Republic of China*
[10]*G.I. Budker Institute of Nuclear Physics SB RAS (BINP), Novosibirsk 630090, Russia*
[11]*GSI Helmholtzcentre for Heavy Ion Research GmbH, D-64291 Darmstadt, Germany*
[12]*Guangxi Normal University, Guilin 541004, People's Republic of China*
[13]*Hangzhou Normal University, Hangzhou 310036, People's Republic of China*
[14]*Helmholtz Institute Mainz, Staudinger Weg 18, D-55099 Mainz, Germany*
[15]*Henan Normal University, Xinxiang 453007, People's Republic of China*
[16]*Henan University of Science and Technology, Luoyang 471003, People's Republic of China*
[17]*Henan University of Technology, Zhengzhou 450001, People's Republic of China*
[18]*Huangshan College, Huangshan 245000, People's Republic of China*
[19]*Hunan Normal University, Changsha 410081, People's Republic of China*
[20]*Hunan University, Changsha 410082, People's Republic of China*
[21]*Indian Institute of Technology Madras, Chennai 600036, India*
[22]*Indiana University, Bloomington, Indiana 47405, USA*
[23a]*INFN Laboratori Nazionali di Frascati, I-00044 Frascati, Italy*
[23b]*INFN Sezione di Perugia, I-06100 Perugia, Italy*
[23c]*University of Perugia, I-06100 Perugia, Italy*
[24a]*INFN Sezione di Ferrara, I-44122 Ferrara, Italy*
[24b]*University of Ferrara, I-44122 Ferrara, Italy*
[25]*Institute of Modern Physics, Lanzhou 730000, People's Republic of China*
[26]*Institute of Physics and Technology, Peace Avenue 54B, Ulaanbaatar 13330, Mongolia*
[27]*Jilin University, Changchun 130012, People's Republic of China*
[28]*Johannes Gutenberg University of Mainz, Johann-Joachim-Becher-Weg 45, D-55099 Mainz, Germany*
[29]*Joint Institute for Nuclear Research, 141980 Dubna, Moscow region, Russia*
[30]*Justus-Liebig-Universitaet Giessen, II. Physikalisches Institut, Heinrich-Buff-Ring 16, D-35392 Giessen, Germany*
[31]*Lanzhou University, Lanzhou 730000, People's Republic of China*
[32]*Liaoning Normal University, Dalian 116029, People's Republic of China*
[33]*Liaoning University, Shenyang 110036, People's Republic of China*
[34]*Nanjing Normal University, Nanjing 210023, People's Republic of China*
[35]*Nanjing University, Nanjing 210093, People's Republic of China*
[36]*Nankai University, Tianjin 300071, People's Republic of China*
[37]*National Centre for Nuclear Research, Warsaw 02-093, Poland*
[38]*North China Electric Power University, Beijing 102206, People's Republic of China*
[39]*Peking University, Beijing 100871, People's Republic of China*
[40]*Qufu Normal University, Qufu 273165, People's Republic of China*
[41]*Shandong Normal University, Jinan 250014, People's Republic of China*
[42]*Shandong University, Jinan 250100, People's Republic of China*

[43]*Shanghai Jiao Tong University, Shanghai 200240, People's Republic of China*
[44]*Shanxi Normal University, Linfen 041004, People's Republic of China*
[45]*Shanxi University, Taiyuan 030006, People's Republic of China*
[46]*Sichuan University, Chengdu 610064, People's Republic of China*
[47]*Soochow University, Suzhou 215006, People's Republic of China*
[48]*South China Normal University, Guangzhou 510006, People's Republic of China*
[49]*Southeast University, Nanjing 211100, People's Republic of China*
[50]*State Key Laboratory of Particle Detection and Electronics, Beijing 100049, Hefei 230026, People's Republic of China*
[51]*Sun Yat-Sen University, Guangzhou 510275, People's Republic of China*
[52]*Suranaree University of Technology, University Avenue 111, Nakhon Ratchasima 30000, Thailand*
[53]*Tsinghua University, Beijing 100084, People's Republic of China*
[54a]*Turkish Accelerator Center Particle Factory Group, Istinye University, 34010, Istanbul, Turkey*
[54b]*Near East University, Nicosia, North Cyprus, Mersin 10, Turkey*
[55]*University of Chinese Academy of Sciences, Beijing 100049, People's Republic of China*
[56]*University of Groningen, NL-9747 AA Groningen, Netherlands*
[57]*University of Hawaii, Honolulu, Hawaii 96822, USA*
[58]*University of Jinan, Jinan 250022, People's Republic of China*
[59]*University of Manchester, Oxford Road, Manchester, M13 9PL, United Kingdom*
[60]*University of Minnesota, Minneapolis, Minnesota 55455, USA*
[61]*University of Muenster, Wilhelm-Klemm-Street 9, 48149 Muenster, Germany*
[62]*University of Oxford, Keble Road, Oxford, United Kingdom OX13RH*
[63]*University of Science and Technology Liaoning, Anshan 114051, People's Republic of China*
[64]*University of Science and Technology of China, Hefei 230026, People's Republic of China*
[65]*University of South China, Hengyang 421001, People's Republic of China*
[66]*University of the Punjab, Lahore-54590, Pakistan*
[67a]*University of Turin and INFN, University of Turin, I-10125 Turin, Italy*
[67b]*University of Eastern Piedmont, I-15121 Alessandria, Italy*
[67c]*INFN, I-10125 Turin, Italy*
[68]*Uppsala University, Box 516, SE-75120 Uppsala, Sweden*
[69]*Wuhan University, Wuhan 430072, People's Republic of China*
[70]*Xinyang Normal University, Xinyang 464000, People's Republic of China*
[71]*Yunnan University, Kunming 650500, People's Republic of China*
[72]*Zhejiang University, Hangzhou 310027, People's Republic of China*
[73]*Zhengzhou University, Zhengzhou 450001, People's Republic of China*

(Received 24 January 2022; accepted 11 March 2022; published 18 April 2022)

Using a sample of $(10.09 \pm 0.04) \times 10^9$ J/ψ events collected with the BESIII detector, a partial wave analysis of $J/\psi \to \gamma\eta'\eta'$ is performed. The masses and widths of the observed resonances and their branching fractions are reported. The main contribution is from $J/\psi \to \gamma f_0(2020)$ with

[a]Also at the Moscow Institute of Physics and Technology, Moscow 141700, Russia.
[b]Also at the Novosibirsk State University, Novosibirsk, 630090, Russia.
[c]Also at the NRC "Kurchatov Institute", PNPI, 188300, Gatchina, Russia.
[d]Also at Goethe University Frankfurt, 60323 Frankfurt am Main, Germany.
[e]Also at Key Laboratory for Particle Physics, Astrophysics and Cosmology, Ministry of Education; Shanghai Key Laboratory for Particle Physics and Cosmology; Institute of Nuclear and Particle Physics, Shanghai 200240, People's Republic of China.
[f]Also at Key Laboratory of Nuclear Physics and Ion-beam Application (MOE) and Institute of Modern Physics, Fudan University, Shanghai 200443, People's Republic of China.
[g]Also at Harvard University, Department of Physics, Cambridge, Massachusetts 02138, USA.
[h]Also at State Key Laboratory of Nuclear Physics and Technology, Peking University, Beijing 100871, People's Republic of China.
[i]Also at School of Physics and Electronics, Hunan University, Changsha 410082, China.
[j]Also at Guangdong Provincial Key Laboratory of Nuclear Science, Institute of Quantum Matter, South China Normal University, Guangzhou 510006, China.
[k]Also at Frontiers Science Center for Rare Isotopes, Lanzhou University, Lanzhou 730000, People's Republic of China.
[l]Also at Lanzhou Center for Theoretical Physics, Lanzhou University, Lanzhou 730000, People's Republic of China.
[m]Henan University of Technology, Zhengzhou 450001, People's Republic of China.

$f_0(2020) \to \eta'\eta'$, which is found with a significance of greater than 25σ. The product branching fraction $\mathcal{B}(J/\psi \to \gamma f_0(2020)) \cdot \mathcal{B}(f_0(2020) \to \eta'\eta')$ is measured to be $(2.63 \pm 0.06(\text{stat.})^{+0.31}_{-0.46}(\text{syst.})) \times 10^{-4}$.

DOI: 10.1103/PhysRevD.105.072002

I. INTRODUCTION

Due to the non-Abelian structure of quantum chromodynamics (QCD), bound states beyond those in the constituent quark model, such as glueballs, which are formed by gluons, are expected [1–3]. The identification of glueballs would provide validation for the quantitative understanding of QCD, and the study of glueballs thus plays an important role in the field of hadron physics. However, possible mixing of pure glueballs with nearby $q\bar{q}$ nonet mesons makes the identification of glueballs difficult both experimentally and theoretically. The radiative J/ψ decay is a gluon-rich process and is therefore regarded as one of the most promising hunting grounds for glueballs [4,5]. Searching for glueballs in $J/\psi \to \gamma\eta'\eta'$, a decay mode which has not been previously explored, is essential.

The spectrum of glueballs is predicted by quenched lattice QCD (LQCD) with the lightest candidate having scalar quantum numbers 0^{++} and a mass in the range of 1.5–1.7 GeV/c^2 with its first excitation at a mass of around 2.6 GeV/c^2 [6–10]. In the partial wave analyses (PWA) of $J/\psi \to \gamma\eta\eta$ [11] and $J/\psi \to \gamma K^0_S K^0_S$ [12], the production rate of $f_0(1710)$ is 1 order of magnitude larger than that of $f_0(1500)$. Referring to the measurements of radiative decays of J/ψ to two mesons listed by the Particle Data Group (PDG) [13], the expected decay rate of $J/\psi \to \gamma f_0(1710)$ is larger than 2.1×10^{-3}, which is comparable to the LQCD prediction of a scalar glueball with rate of 3.8×10^{-3} [14].

The high production rate suggests that the $f_0(1710)$ has a large gluonic component. The copious production of scalar resonances around 2.1 GeV/c^2 has also been reported in $J/\psi \to \gamma\eta\eta$ [11] and $J/\psi \to \gamma K^0_S K^0_S$ [12]. The high production rate of these scalar resonances, which is similar to that of $f_0(1710)$, indicates that the scalars around 2.1 GeV/c^2 may significantly overlap with the first scalar glueball excitation. The decay width of a scalar glueball to $\eta'\eta'$ should be comparable to that of a scalar glueball to $\eta\eta$, considering flavor symmetry. Studies from $p\bar{p}$ annihilation, another gluon-rich process, show that the $f_0(2100)$ has a coupling to $\eta\eta$ stronger than that to $\pi\pi$ [15,16], revealing a strange decay pattern. Searching for scalars around 2.1 GeV/c^2 in $\eta'\eta'$ will help clarify their nature.

The mass of the lightest tensor glueball state is predicted to be 2.3–2.4 GeV/c^2 [7,8], which is consistent with the measurement of the $f_2(2340)$. The $f_2(2340)$ was observed firstly in $\pi^- p \to \phi\phi n$ [17]. It was also observed in $J/\psi \to \gamma\eta\eta$ [11] and $J/\psi \to \gamma\phi\phi$ [18] with large production rates. A significant tensor structure around 2.4 GeV/c^2 was also seen in $J/\psi \to \gamma\pi^0\pi^0$ [19] and $J/\psi \to \gamma K^0_S K^0_S$ [12]. However, the measured production rate of the $f_2(2340)$ in radiative J/ψ decays from existing experimental studies is much lower than that from the LQCD predictions of the tensor glueball [20]. Studies of more decay modes of the $f_2(2340)$ are desirable.

In this paper, the result of a partial wave analysis of $J/\psi \to \gamma\eta'\eta'$ is presented based on a sample of $10.09 \times 10^9 J/\psi$ events [21] collected with the BESIII detector. The two η' are reconstructed using their decays to $\gamma\pi^+\pi^-$ or $\eta(\to \gamma\gamma)\pi^+\pi^-$. Two combinations of η' decays are used to reconstruct $J/\psi \to \gamma\eta'\eta'$: in the first, called mode I, both η' are from $\eta\pi^+\pi^-$; in the second, mode II, one η' decays to $\gamma\pi^+\pi^-$ and the other η' decays to $\eta\pi^+\pi^-$.

II. DETECTOR AND MONTE CARLO SIMULATIONS

The BESIII detector [22] records symmetric e^+e^- collisions provided by the BEPCII storage ring with a designed peak luminosity of 1×10^{33} cm^{-2} s^{-1} in the center-of-mass energy range from 2.0 to 4.9 GeV. BESIII has collected large data samples in this energy region [23]. The cylindrical core of the BESIII detector covers 93% of the full solid angle and consists of a helium-based multilayer drift chamber (MDC), a plastic scintillator time-of-flight system (TOF), and a CsI(Tl) electromagnetic calorimeter (EMC), which are all enclosed in a superconducting solenoidal magnet providing a 1.0 T (0.9 T in 2012) magnetic field. The solenoid is supported by an octagonal flux-return yoke with resistive plate counter muon identification modules interleaved with steel. The charged-particle momentum resolution at 1 GeV/c is 0.5%, and the dE/dx resolution is 6% for electrons from Bhabha scattering. The EMC measures photon energies with a resolution of 2.5% (5%) at 1 GeV in the barrel (end cap) region. The time resolution in the TOF barrel region is 68 ps, while that in the end cap region was initially 110 ps. The end cap TOF system was upgraded in 2015 with multigap resistive plate chamber technology, improving the time resolution to be 60 ps [24].

Simulated data samples produced with a GEANT4-based [25] Monte Carlo (MC) package, which includes the geometric description of the BESIII detector and the detector response, are used to determine detection efficiencies and to estimate backgrounds. The simulation models the beam energy spread and initial state radiation (ISR) in the e^+e^- annihilations with the generator KKMC [26].

The inclusive MC sample includes both the production of the J/ψ resonance and the continuum processes incorporated in KKMC [26]. The known decay modes are modeled with EVTGEN [27] using branching fractions taken from the PDG [13], and the remaining unknown charmonium decays are modeled with LUNDCHARM [28]. Final state radiation (FSR) from charged final state particles is incorporated using the PHOTOS package [29].

To estimate the detection efficiency and to optimize the selection criteria, signal MC events are generated for $J/\psi \to \gamma\eta'\eta'$ in mode I and II. The process $\eta' \to \gamma\pi^+\pi^-$ is simulated taking into account both the $\rho - \omega$ interference and the box anomaly [30]. The remaining processes excluding $\eta' \to \gamma\pi^+\pi^-$ are simulated using a phase-space (PHSP) generator. Based on studies of Bhabha, dimuon and inclusive hadronic event samples, the trigger efficiency for events with charged tracks is found to be approximately 100% [31,32] and is thus neglected in this analysis.

III. EVENT SELECTION

Charged tracks detected in the MDC are required to be within a polar angle (θ) range of $|\cos\theta| < 0.93$, where θ is defined with respect to the z-axis. The distance of closest approach to the interaction point (IP) must be less than 10 cm along the z-axis, $|V_z|$, and less than 1 cm in the transverse plane, $|V_{xy}|$. Particle identification (PID) for charged tracks combines measurements of the energy deposited in the MDC (dE/dx) and the flight time in the TOF to form likelihoods $\mathcal{L}(h)(h = p, K, \pi)$ for each hadron h hypothesis. Each track is assigned to the particle type corresponding to the highest likelihoods. Candidate events are required to have four charged π tracks and zero net charge. Photon candidates are identified using showers in the EMC. The deposited energy of each shower must be more than 25 MeV in the barrel region ($|\cos\theta| < 0.80$) and more than 50 MeV in the end cap region ($0.86 < |\cos\theta| < 0.92$). To exclude showers that originate from charged tracks, the angle between the position of each shower in the EMC and the closest extrapolated charged track must be greater than 10°. To suppress electronic noise and showers unrelated to the event, the difference between the EMC time and the event start time is required to be within (0, 700) ns.

In mode I, with $J/\psi \to \gamma\eta'\eta'$, $\eta' \to \eta\pi^+\pi^-$, and $\eta \to \gamma\gamma$, the final state consists of 5γ and $2(\pi^+\pi^-)$. To reduce background events and improve mass resolution, a six-constraint (6C) kinematic fit is performed under the hypothesis of $J/\psi \to \gamma\eta\eta\pi^+\pi^-\pi^+\pi^-$ imposing energy-momentum conservation (4C) and constraining the mass of each pair of photons to the nominal mass of η [13]. For events with more than one combination of $J/\psi \to \gamma\eta\eta\pi^+\pi^-\pi^+\pi^-$, the combination with the least $\chi^2_{\rm 6C}$ is selected, and $\chi^2_{\rm 6C} < 85$ is required. To suppress background contributions with one more or one less photon, four-constraint kinematic fits are performed separately under the hypotheses of $J/\psi \to 4\gamma\pi^+\pi^-\pi^+\pi^-$, $J/\psi \to 5\gamma\pi^+\pi^-\pi^+\pi^-$, $J/\psi \to 6\gamma\pi^+\pi^-\pi^+\pi^-$, whose χ^2 values are denoted as $\chi^2_{4\gamma}, \chi^2_{5\gamma}, \chi^2_{6\gamma}$, respectively. Events with $\chi^2_{5\gamma} < \chi^2_{4\gamma}$ and $\chi^2_{5\gamma} < \chi^2_{6\gamma}$ are accepted. Two η' candidates are reconstructed from the $\eta\pi^+\pi^-$ combinations with the least $|M_{(\eta\pi^+\pi^-)_1} - m_{\eta'}|^2 + |M_{(\eta\pi^+\pi^-)_2} - m_{\eta'}|^2$, where $M_{(\eta\pi^+\pi^-)_{1,2}}$ are the invariant masses of different $\eta\pi^+\pi^-$ combinations and $m_{\eta'}$ is the nominal mass of the η' [13]. The η' candidates are then selected with $|M_{\eta\pi^+\pi^-} - m_{\eta'}| < 0.01$ GeV/c^2. Here, the two η' candidates are denoted as η'_1 and η'_2, based on the absolute value of their momenta, for which $|\vec{p}_{\eta'_1}| > |\vec{p}_{\eta'_2}|$. A clear η' signal is observed in the invariant mass distribution of $\eta\pi^+\pi^-$ ($M_{\eta\pi^+\pi^-}$), as shown in Fig. 1(a). The distribution of the two $M_{\eta\pi^+\pi^-}$ of the remaining events is shown in Fig. 2(a), where the signal region is the red box labeled as "0."

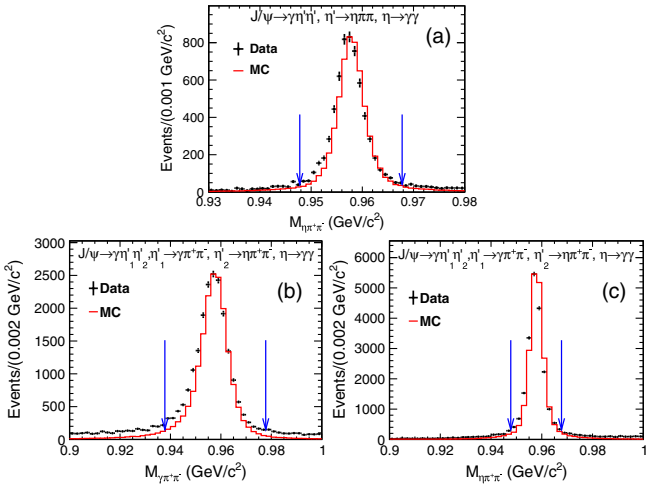

FIG. 1. Invariant mass distributions of (a) $M_{\eta\pi^+\pi^-}$ in mode I, and (b) $M_{\gamma\pi^+\pi^-}$, (c) $M_{\eta\pi^+\pi^-}$ in mode II for the selected candidates. The dots with error bars are data, and the histograms depict the signal MC samples (normalized by height).

In mode II, with $J/\psi \to \gamma\eta'_1\eta'_2$, $\eta'_1 \to \gamma\pi^+\pi^-$, $\eta'_2 \to \eta\pi^+\pi^-$, and $\eta \to \gamma\gamma$, the final state consists of 4γ and $2(\pi^+\pi^-)$. The subscripts (1, 2) correspond to the different decay modes of η'. A five-constraint (5C) kinematic fit is performed under the hypothesis of $J/\psi \to \gamma\gamma\eta\pi^+\pi^-\pi^+\pi^-$. In case of more than one combination, the one with the least $\chi^2_{\rm 5C}$ is retained, and the condition $\chi^2_{\rm 5C} < 75$ is required. To suppress background contributions with one more or one less photon, four-constraint kinematic fits are performed separately under the hypotheses of $J/\psi \to 3\gamma\pi^+\pi^-\pi^+\pi^-$, $J/\psi \to 4\gamma\pi^+\pi^-\pi^+\pi^-$, $J/\psi \to 5\gamma\pi^+\pi^-\pi^+\pi^-$, whose χ^2 values are denoted as $\chi^{2\prime}_{3\gamma}, \chi^{2\prime}_{4\gamma}, \chi^{2\prime}_{5\gamma}$, respectively. Events with $\chi^{2\prime}_{4\gamma} < \chi^{2\prime}_{3\gamma}$ and $\chi^{2\prime}_{4\gamma} < \chi^{2\prime}_{5\gamma}$ are accepted. To suppress background due to $\pi^0 \to \gamma\gamma$, $|M_{\gamma\gamma} - m_{\pi^0}| > 0.02$ GeV/c^2 is required for all possible two-photon combinations excluding the one forming the η, where m_{π^0} is the nominal mass of the π^0. Invariant mass

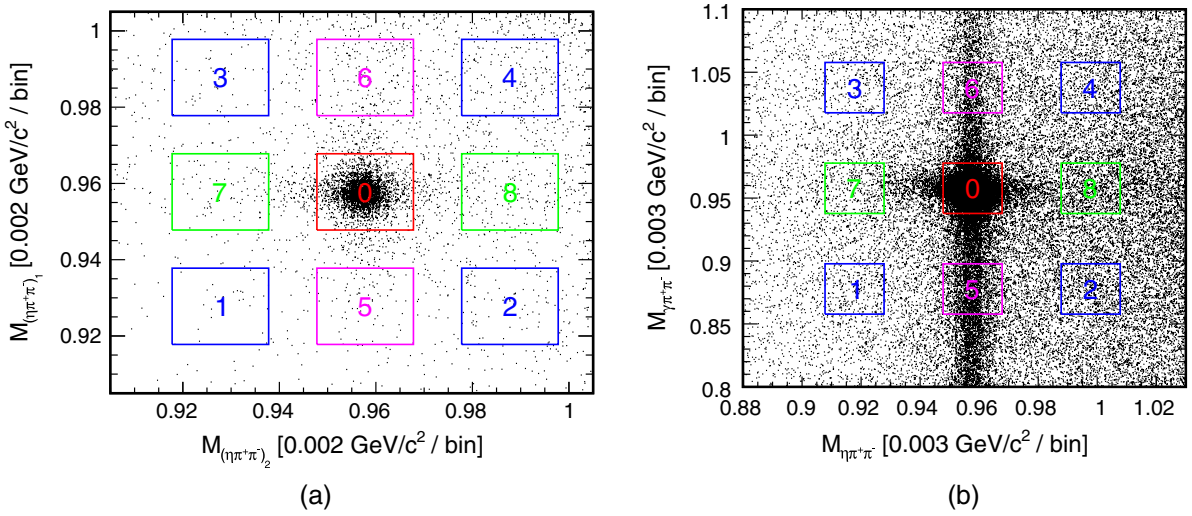

FIG. 2. The distributions of (a) $M_{(\eta\pi^+\pi^-)_1}$ versus $M_{(\eta\pi^+\pi^-)_2}$ in mode I and (b) $M_{\gamma\pi^+\pi^-}$ versus $M_{\eta\pi^+\pi^-}$ in mode II. The red box labeled as "0" and other boxes labeled from "1" to "8" are signal region and sideband regions as defined in the text, respectively.

of the $\pi^+\pi^-$ in $\eta' \to \gamma\pi^+\pi^-$ is required to be within the ρ mass region, $0.4\ \mathrm{GeV}/c^2 < M_{\pi^+\pi^-} < 0.85\ \mathrm{GeV}/c^2$. The η' candidates are formed from the $\gamma\pi^+\pi^-$ and $\eta\pi^+\pi^-$ combination with the least $\frac{|M_{\gamma\pi^+\pi^-}-m_{\eta'}|^2}{\sigma^2_{\gamma\pi^+\pi^-}} + \frac{|M_{\eta\pi^+\pi^-}-m_{\eta'}|^2}{\sigma^2_{\eta\pi^+\pi^-}}$ and are then selected with $|M_{\gamma\pi^+\pi^-} - m_{\eta'}| < 0.02\ \mathrm{GeV}/c^2$, $|M_{\eta\pi^+\pi^-} - m_{\eta'}| < 0.01\ \mathrm{GeV}/c^2$. Here, $M_{\gamma\pi^+\pi^-}$ and $M_{\eta\pi^+\pi^-}$ are the invariant masses of $\gamma\pi^+\pi^-$ and $\eta\pi^+\pi^-$, as shown in Figs. 1(b) and 1(c); $\sigma_{\gamma\pi^+\pi^-}$ and $\sigma_{\eta\pi^+\pi^-}$ are the invariant mass resolutions of $\gamma\pi^+\pi^-$ and $\eta\pi^+\pi^-$, which are determined to be 6.8 MeV/c^2 and 3.4 MeV/c^2 from fitting with a double Gaussian function plus a first order polynomial function to the individual distributions. To suppress backgrounds introduced by fake photons, such as $J/\psi \to \pi^+\pi^-\pi^0\eta'$, $M_{\eta'\eta'} < 3.0\ \mathrm{GeV}/c^2$ is required. The distribution of $M_{\gamma\pi^+\pi^-}$ versus $M_{\eta\pi^+\pi^-}$ of the remaining events is shown in Fig. 2(b), where the red box labeled as "0" shows the signal region.

After applying the requirements above, 3081 and 19866 events survived for mode I, II, respectively. The invariant mass distribution of $\eta'\eta'$ ($M_{\eta'\eta'}$) and the Dalitz plot for these two modes are shown in Figs. 3 and 4.

No background events with $\eta'\eta'$ in the final state are observed in these two decay modes in a study using a MC sample of 10.01×10^9 J/ψ inclusive decays with a generic event type analysis tool [33]. Non-$\eta'\eta'$ backgrounds are estimated using the $\eta'\eta'$ sideband events from data. The two-dimensional sidebands for these two modes are illustrated by solid boxes labeled from "1" to "8" in Fig. 2, where the sideband regions are defined as $0.02\ \mathrm{GeV}/c^2 \le |M_{\eta\pi^+\pi^-(1,2)} - m_{\eta'}| \le 0.04\ \mathrm{GeV}/c^2$ for mode I and $0.06\ \mathrm{GeV}/c^2 \le |M_{\gamma\pi^+\pi^-} - m_{\eta'}| \le 0.10\ \mathrm{GeV}/c^2$, $0.03\ \mathrm{GeV}/c^2 \le |M_{\eta\pi^+\pi^-} - m_{\eta'}| \le 0.05\ \mathrm{GeV}/c^2$ for mode II, respectively. The shaded histograms in Figs. 3(a) and 3(b) show the background contributions from the

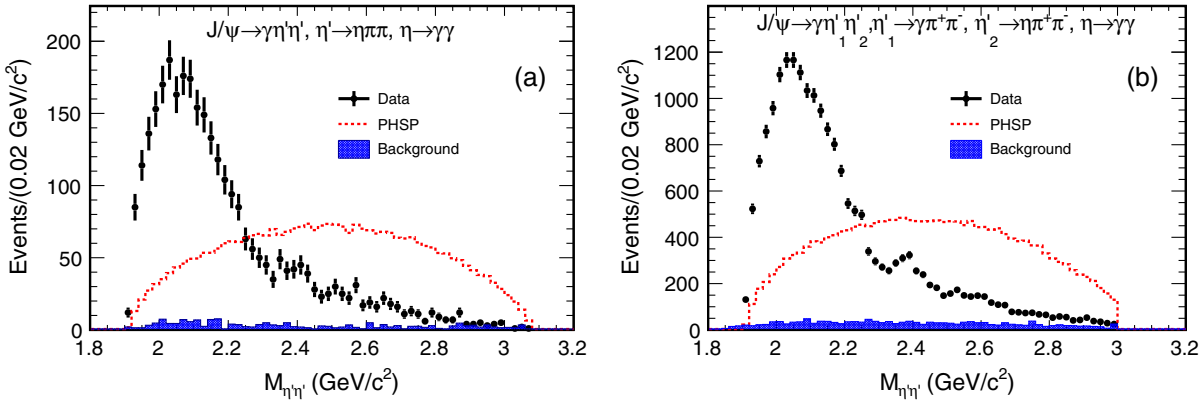

FIG. 3. Invariant mass distributions of $M_{\eta'\eta'}$ in (a) mode I and (b) mode II for the selected $\gamma\eta'\eta'$ candidates. The points with error bars and the dashed line show data and the signal PHSP MC samples (normalized by integral), respectively; the shaded histograms show the background contributions estimated from $\eta'\eta'$ sidebands.

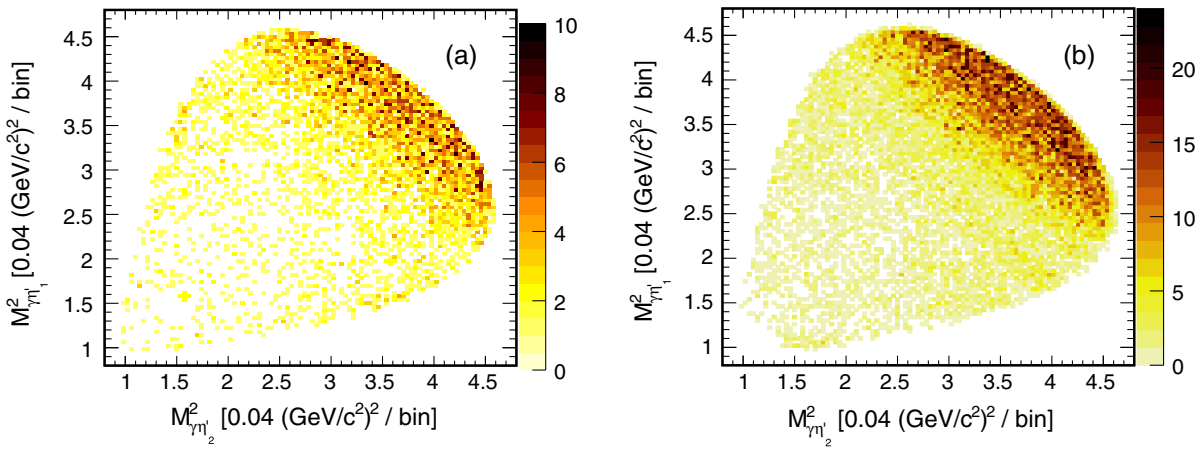

FIG. 4. Dalitz plots for the selected candidates in (a) mode I and (b) mode II.

normalized sideband events in mode I and mode II, where the numbers of events are 175 and 1576, respectively, corresponding to background fractions of 5.7% and 7.9%.

IV. PARTIAL WAVE ANALYSIS

A. Analysis method

A PWA is performed to disentangle the structures present in $J/\psi \to \gamma\eta'\eta'$ decays using the GPUPWA framework [34]. The quasi two-body decay amplitudes in the sequential decay processes $J/\psi \to \gamma X$, $X \to \eta'\eta'$ and $J/\psi \to \eta' X$, $X \to \gamma\eta'$ are constructed using covariant tensor amplitudes described in Ref. [35]. For radiative and hadronic J/ψ decays to mesons, the general forms for covariant tensor amplitudes A are formulated as

$$A = \psi_\mu(m_1) e^*_\nu(m_2) A^{\mu\nu} = \psi_\mu(m_1) e^*_\nu(m_2) \sum_i \Lambda_i U_i^{\mu\nu}, \quad (1)$$

and

$$A = \psi_\mu(m) A^\mu = \psi_\mu(m) \sum_i \Lambda_i U_i^\mu, \quad (2)$$

respectively, according to Ref. [35], where $\psi_\mu(m_1)$ is the J/ψ polarization four-vector, $e_\mu(m_2)$ is the polarization vector of the photon and $U_i^{\mu\nu}(U_i^\mu)$ is the partial wave amplitude with a coupling strength determined by the complex parameter Λ_i. The partial wave amplitudes U_i for the intermediate states used in the analysis are constructed with the four-momenta of the particles in the final states, and their specific expressions are given in Ref. [35].

Each intermediate resonance X is parametrized by a constant-width, relativistic Breit-Wigner (BW) propagator,

$$BW(s) = \frac{1}{M^2 - s - iM\Gamma}, \quad (3)$$

where s is the invariant mass squared of $\eta'\eta'$ or $\gamma\eta'$, and M, Γ are the mass and width of the intermediate resonance.

The complex parameters of the amplitudes and resonance parameters are determined by an unbinned maximum likelihood fit. The probability to observe the ith event characterized by the measurement ξ, i.e., the measured four-momenta of the particles in the final states, is

$$P(\xi_i) = \frac{\omega(\xi_i)\varepsilon(\xi_i)}{\int d\xi \omega(\xi)\varepsilon(\xi)}, \quad (4)$$

where $\varepsilon(\xi)$ is the detection efficiency, $\omega(\xi_i) \equiv (\frac{d\sigma}{d\Phi})_i$ is the differential cross section, and $d\Phi$ is the standard element of phase space. The differential cross section is

$$\frac{d\sigma}{d\Phi} = \left| \sum A(J^{PC}) \right|^2, \quad (5)$$

where $A(J^{PC})$ is the amplitude for all possible intermediate resonances with spin-parity J^{PC}. $\int d\xi \omega(\xi)\varepsilon(\xi) \equiv \sigma'$ is the measured yields.

The likelihood for observing the N events in the data sample is

$$\mathcal{L} = \prod_{i=1}^{N} P(\xi_i) = \prod_{i=1}^{N} \frac{(\frac{d\sigma}{d\Phi})_i \cdot \varepsilon(\xi_i)}{\sigma'}. \quad (6)$$

For technical reasons, rather than maximizing $\mathcal{L}$, $-\ln\mathcal{L}$ is minimized, i.e.,

$$-\ln\mathcal{L} = -\sum_{i=1}^{N} \ln\left(\frac{(\frac{d\sigma}{d\Phi})_i}{\sigma'}\right) - \sum_{i=1}^{N} \ln\varepsilon(\xi_i) \quad (7)$$

for a given data set. The second term is a constant and has no impact on the determination of the parameters or on the related changes of $-\ln\mathcal{L}$, which is then defined as

$$-\ln\mathcal{L} = -\sum_{i=1}^{N} \ln\left(\frac{(\frac{d\sigma}{d\Phi})_i}{\sigma'}\right) = -\sum_{i=1}^{N} \ln\left(\frac{d\sigma}{d\Phi}\right)_i + N\ln\sigma' \quad (8)$$

in the fitting. The free parameters are optimized by using MINUIT [36]. The measured yields σ' is evaluated using MC techniques. An MC sample of $N_{\rm gen}$ is generated with signal events that are uniformly distributed in phase space. These events are subjected to the event selection criteria and yield a sample of $N_{\rm acc}$ accepted events. The normalization integral is computed as

$$\int \mathrm{d}\xi\omega(\xi)\varepsilon(\xi) = \sigma' \to \frac{1}{N_{\rm gen}}\sum_{k}^{N_{\rm acc}}\left(\frac{\mathrm{d}\sigma}{\mathrm{d}\Phi}\right)_k. \tag{9}$$

To take into account the non-$\eta'\eta'$ background contribution in data, the negative log-likelihood (NLL) value obtained from events in the $\eta'\eta'$ signal region is subtracted by the NLL value obtained from events in the $\eta'\eta'$ sideband regions, i.e.,

$$-\ln\mathcal{L}_{\rm sig} = -\left(\ln\mathcal{L}_{\rm data} - \sum_i \omega_i\cdot\ln\mathcal{L}_{{\rm bkg}_i}\right), \tag{10}$$

where ω_i represents the scaling factor of background events in different $\eta'\eta'$ sideband region, and $\mathcal{L}_{{\rm bkg}_i}$ means the likelihood from corresponding background events.

The number of fitted events N_X for an intermediate resonance X, which has N_{W_X} independent partial wave amplitudes A_j, is defined as

$$N_X = \frac{\sigma_X}{\sigma'}\cdot N', \tag{11}$$

where N' is the number of selected events after background subtraction and

$$\sigma_X = \frac{1}{N_{\rm gen}}\sum_{k}^{N_{\rm acc}}\left|\sum_{j}^{N_{W_X}}(A_j)_k\right|^2 \tag{12}$$

is the measured cross section of the resonance X and is calculated with the same MC sample as the measured total cross section σ'. The detection efficiency ε_X is obtained by the partial wave amplitude weighted MC sample,

$$\varepsilon_X = \frac{\sigma_X}{\sigma_X^{\rm gen}} = \frac{\sum_k^{N_{\rm acc}}|\sum_j^{N_{W_X}}(A_j)_k|^2}{\sum_i^{N_{\rm gen}}|\sum_j^{N_{W_X}}(A_j)_i|^2}. \tag{13}$$

Based on GPUPWA, a combined fit for mode I and II is performed. The combined branching fraction of $J/\psi\to\gamma X$, $X\to\eta'\eta'$ or $J/\psi\to\eta' X$, $X\to\gamma\eta'$ is calculated by

$$\mathcal{B}(J/\psi\to\gamma X \quad \text{or} \quad \eta' X\to\gamma\eta'\eta') = \frac{N_{X_{\rm I}}+N_{X_{\rm II}}}{N_{J/\psi}\cdot\mathcal{B}_{\eta'\to\eta\pi^+\pi^-}\cdot\mathcal{B}_{\eta\to\gamma\gamma}\cdot(\mathcal{B}_{\eta'\to\eta\pi^+\pi^-}\cdot\mathcal{B}_{\eta\to\gamma\gamma}\cdot\varepsilon_{X_{\rm I}}+\mathcal{B}_{\eta'\to\gamma\pi^+\pi^-}\cdot\varepsilon_{X_{\rm II}}\cdot 2)}, \tag{14}$$

where the subscripts (I, II) correspond to mode I and mode II, respectively, $N_{J/\psi}$ is the total number of J/ψ events, and $\mathcal{B}_{\eta'\to\eta\pi^+\pi^-}, \mathcal{B}_{\eta'\to\gamma\pi^+\pi^-}, \mathcal{B}_{\eta\to\gamma\gamma}$ are the branching fractions of $\eta'\to\eta\pi^+\pi^-$, $\eta'\to\gamma\pi^+\pi^-$, $\eta\to\gamma\gamma$ from Ref. [13], respectively. The factor 2 in the second term of the denominator in Eq. (14) represents the combination of the two decay modes of η'.

B. PWA results

In this analysis, all combinations of possible resonances in the PDG [13] and Ref. [37] with $J^{PC}=0^{++},2^{++},4^{++}$ in $\eta'\eta'$ and $J^{PC}=1^{+-},1^{--}$ in $\gamma\eta'$ are considered, as listed in Table I. Because of centrifugal barriers, production of $\gamma\eta'$ intermediate states with $J\geq 3$ and of $\eta'\eta'$ intermediate states with $J\geq 6$ in $J/\psi\to\gamma\eta'\eta'$ is not considered. Changes in the NLL value and the number of free

TABLE I. States considered in this analysis with $J^{PC}=0^{++},2^{++},4^{++}$ in $\eta'\eta'$ and $J^{PC}=1^{+-},1^{--}$ in $\gamma\eta'$ and the significances of additional resonances. "*" means the state is from Ref. [37]. PHSP means the nonresonant contribution.

	State	J^{PC}	Significance (σ)
Baseline model	0^{++} PHSP	0^{++}	···
	$f_0(2020)$	0^{++}	···
	$f_0(2330)$	0^{++}	···
	$f_2(2340)$	2^{++}	···
	$h_1(1415)$	1^{+-}	···

(Table continued)

TABLE I. *(Continued)*

	State	J^{PC}	Significance (σ)
Additional states	$f_0(2020)^*$	0^{++}	0.0
	$f_0(2060)$	0^{++}	0.0
	$f_0(2100)$	0^{++}	0.0
	$f_0(2102)^*$	0^{++}	0.0
	$f_0(2200)$	0^{++}	0.1
	2^{++} PHSP	2^{++}	1.1
	$f_2(1910)$	2^{++}	0.9
	$f_2(1934)^*$	2^{++}	0.4
	$f_2(1950)$	2^{++}	0.2
	$f_2(2000)$	2^{++}	0.4
	$f_2(2010)$	2^{++}	0.9
	$f_2(2010)^*$	2^{++}	0.0
	$f_2(2140)$	2^{++}	0.7
	$f_2(2150)$	2^{++}	0.0
	$f_2(2220)$	2^{++}	1.4
	$f_2(2240)$	2^{++}	0.2

(Table continued)

TABLE I. *(Continued)*

State	J^{PC}	Significance (σ)
$f_2(2295)$	2^{++}	0.3
$f_2(2300)$	2^{++}	0.9
4^{++} PHSP	4^{++}	0.7
$f_4(2018)^*$	4^{++}	0.2
$f_4(2050)$	4^{++}	0.2
$f_4(2220)$	4^{++}	0.0
$X(2260)$	4^{++}	0.5
$f_4(2283)^*$	4^{++}	0.6
$f_4(2300)$	4^{++}	0.5
1^{+-} PHSP	1^{+-}	1.8
$h_1(1170)$	1^{+-}	2.3
$h_1(1595)$	1^{+-}	0.2
1^{--} PHSP	1^{--}	0.1
$\omega(1420)$	1^{--}	0.5
$\omega(1650)$	1^{--}	0.1
$\phi(1680)$	1^{--}	0.4
$\phi(2170)$	1^{--}	2.0
$\rho(1450)$	1^{--}	0.0
$\rho(1570)$	1^{--}	0.6
$\rho(1700)$	1^{--}	0.2
$\rho(1900)$	1^{--}	2.4
$\rho(2150)$	1^{--}	0.9

parameters in the fit with and without a resonance are used to evaluate its statistical significance. All components with significance greater than 5σ are retained in the baseline model. The baseline model contains two 0^{++} resonances [$f_0(2020)$, $f_0(2330)$], one 2^{++} resonance [$f_2(2340)$], one 1^{+-} resonance [$h_1(1415)$], and the nonresonant decay of $J/\psi \to \gamma\eta'\eta'$, which is modeled by a 0^{++} phase space distribution (0^{++} PHSP) of the $\eta'\eta'$ system. In the high energy region of the $\eta'\eta'$ spectrum, a new scalar, $f_0(2480)$, is needed to describe data with a significance of 6.0σ. By taking into account the look-elsewhere effect [38], the significance is 5.2σ. Additional resonances listed in Table I are tested. None of them has a statistical significance larger than 5σ. The existence of possible additional resonances is further studied by performing scans for extra resonances ($J^{PC} = 0^{++}, 2^{++}, 4^{++}, 1^{+-}, 1^{--}$) with different masses and widths. The scan results yield no evidence for extra intermediate states. The masses and widths of all resonances in the baseline model, product branching fractions of $J/\psi \to \gamma X$, $X \to \eta'\eta'$ or $J/\psi \to \eta' X$, $X \to \gamma\eta'$, and the statistical significances are summarized in Table II, where the first uncertainties are statistical and the second are systematic. The fit fraction of each component and their interference fractions are listed in Table III. The comparisons of data and the PWA fit projection (weighted by MC efficiencies) of the invariant mass distributions of $\eta'\eta'$ and $\gamma\eta'$ for the fitted parameters are shown in Figs. 5(a) and 5(b). To make the components with small fit fractions [the $f_0(2480)$ and the $h_1(1415)$] visible, the zoomed view of these two distributions in logarithm scale are shown in Figs. 5(c) and 5(d). The comparisons of the projected data and MC angular distributions are shown in Figs. 5(e)–5(g). The $\chi^2/N_{\rm bins}$ value is displayed on each figure to demonstrate the goodness of fit, where $N_{\rm bins}$ is the number of bins of each figure and the χ^2 is defined as

TABLE II. Mass, width, $\mathcal{B}(J/\psi \to \gamma X \to \gamma\eta'\eta')$ or $\mathcal{B}(J/\psi \to \eta' X \to \gamma\eta'\eta')$ branching fraction (B.F.) and significance of each component in the baseline model. The first uncertainties are statistical and the second are systematic.

Resonance	M(MeV/c^2)	Γ(MeV)	B.F.	Significance (σ)
$f_0(2020)$	$1982 \pm 3^{+54}_{-0}$	$436 \pm 4^{+46}_{-49}$	$(2.63 \pm 0.06^{+0.31}_{-0.46}) \times 10^{-4}$	$\gg 25$
$f_0(2330)$	$2312 \pm 2^{+10}_{-0}$	$134 \pm 5^{+30}_{-9}$	$(6.09 \pm 0.64^{+4.00}_{-1.68}) \times 10^{-6}$	16.3
$f_0(2480)$	$2470 \pm 4^{+4}_{-6}$	$75 \pm 9^{+11}_{-8}$	$(8.18 \pm 1.77^{+3.73}_{-2.23}) \times 10^{-7}$	5.2
$h_1(1415)$	$1384 \pm 6^{+9}_{-0}$	$66 \pm 10^{+12}_{-10}$	$(4.69 \pm 0.80^{+0.74}_{-1.82}) \times 10^{-7}$	5.3
$f_2(2340)$	$2346 \pm 8^{+22}_{-6}$	$332 \pm 14^{+26}_{-12}$	$(8.67 \pm 0.70^{+0.61}_{-1.67}) \times 10^{-6}$	16.1
0^{++} PHSP	…	…	$(1.17 \pm 0.23^{+4.09}_{-0.70}) \times 10^{-5}$	15.7

TABLE III. Fraction of each component or interference fractions between two components (%) in the baseline model. The uncertainties are statistical only.

Resonance	$f_0(2020)$	$f_0(2330)$	$f_0(2480)$	$h_1(1415)$	$f_2(2340)$	0^{++} PHSP
$f_0(2020)$	125.0 ± 2.7	-23.7 ± 1.4	-3.3 ± 0.6	0.8 ± 0.3	0.5 ± 0.2	-14.3 ± 1.6
$f_0(2330)$		3.0 ± 0.3	-0.1 ± 0.1	-0.2 ± 0.0	-0.4 ± 0.0	2.9 ± 0.2
$f_0(2480)$			0.4 ± 0.1	0.0 ± 0.0	0.1 ± 0.0	0.0 ± 0.1
$h_1(1415)$				0.2 ± 0.0	0.0 ± 0.1	-1.0 ± 0.1
$f_2(2340)$					5.0 ± 0.4	-0.6 ± 0.1
0^{++} PHSP						5.8 ± 1.1

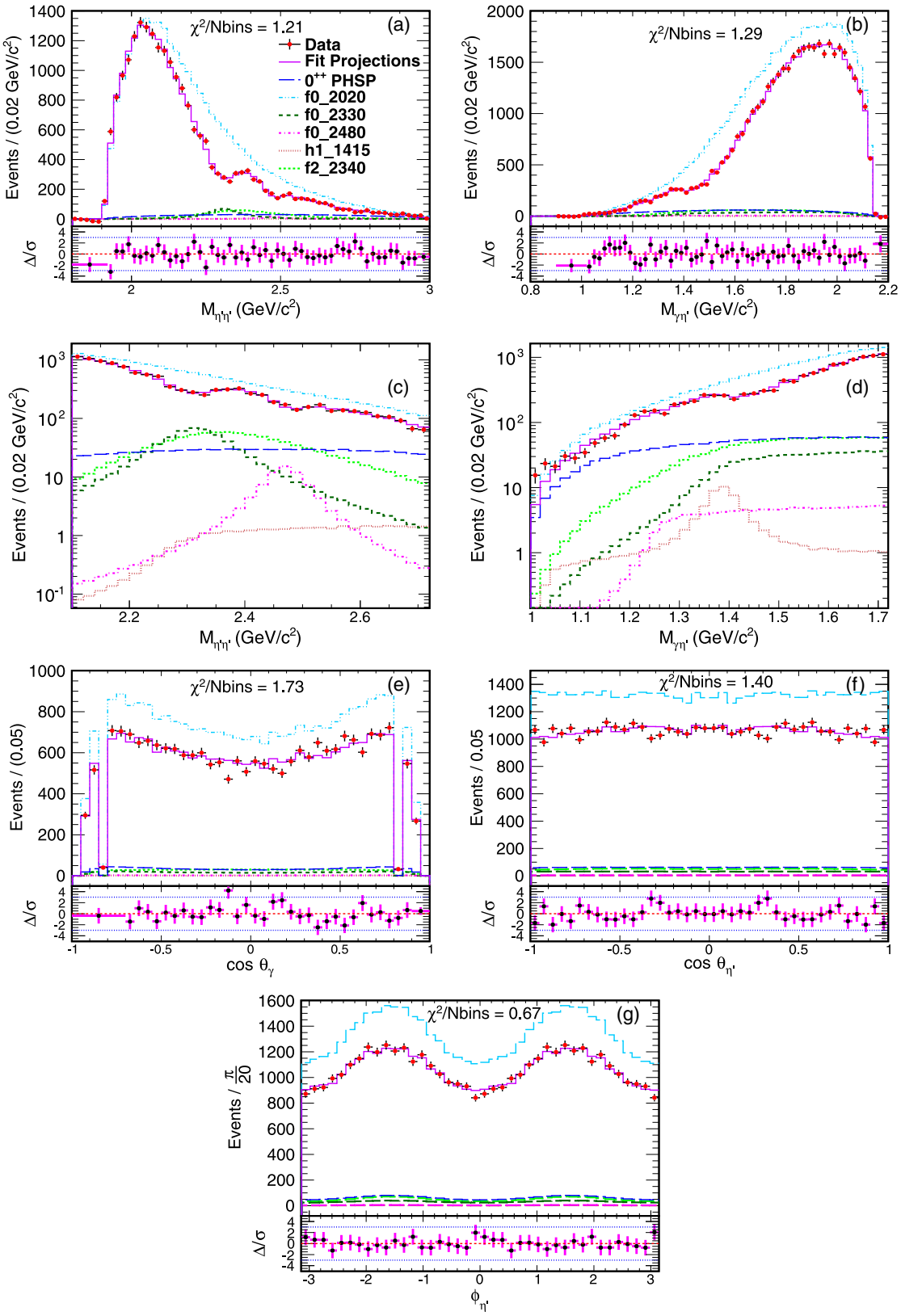

FIG. 5. Superposition of data and the combined PWA fit projections for: Invariant mass distributions of (a) $M_{\eta'\eta'}$, (b) $M_{\gamma\eta'}$ (the bins at the left and right edges in the pull distributions are combined due to low statistics); zoomed view of invariant mass distributions of (c) $M_{\eta'\eta'}$, (d) $M_{\gamma\eta'}$ in logarithm scale; cos θ of (e) γ in the J/ψ rest frame, (f) η' in the $\eta'\eta'$ rest frame; (g) azimuthal angle between the normals to the two decay planes of η' in the $\eta'\eta'$ rest frame.

$$\chi^2 = \sum_{i=1}^{N_{\rm bins}} \frac{(n_i - \nu_i)^2}{\nu_i}, \tag{15}$$

where n_i and ν_i are the number of events for the data and the fit projections with the baseline model in the ith bin of each figure, respectively.

Various checks are performed to verify the reliability of the PWA baseline model. The statistical significance of additional nonresonant contributions with $J^{PC} = 2^{++}, 4^{++}, 1^{+-}$ or 1^{--} is less than 5σ. If 0^{++} PHSP is replaced by 2^{++} or 4^{++} PHSP, the NLL value will be worsened by 116.8 or 123.4. For the scalar around 2.1 GeV/c^2, the fitted mass and width are close to the resonance parameters of the $f_0(2020)$ from the PDG [13]. If its mass and width are fixed to the resonance parameters of $f_0(2100)$ or $f_0(2200)$ in the PDG, the NLL value will be worsened by 324.1 or 1437.2, respectively. Since the $f_0(2020)$ is near the $\eta'\eta'$ threshold and $\eta'\eta'$ is not its dominant decay channel, a mass-dependent-width BW form is used to parametrize the resonance as the following:

$$BW(s) = \frac{1}{M^2 - s - i\sqrt{s}\cdot\Gamma(s)}, \tag{16}$$

with

$$\Gamma(s) = R\cdot\Gamma(M^2)\left(\frac{M^2}{s}\right)\left(\frac{\rho(s)}{\rho(M^2)}\right)^{2l+1} + (1-R)\cdot\Gamma_0, \tag{17}$$

where the first term of $\Gamma(s)$ corresponds to the decay of $f_0(2020) \to \eta'\eta'$, R is the $\mathcal{B}(f_0(2020) \to \eta'\eta')$ which is estimated to be 0.1 from the PDG [13], $\rho(s)$ is the momentum of the η' in the resonance rest frame, Γ_0 is the constant width of the $f_0(2020)$ from the PDG [13]. The difference between the result in the parametrization using a constant-width BW and that of the mass-dependent-width BW is assigned as part of the systematic uncertainties shown in Sec. V. If the J^{PC} of the $f_0(2480)$ is changed from 0^{++} to 2^{++} or 4^{++}, the NLL value will be worsened by 20.3 or 30.2, respectively. The significance of the $f_0(2480)(0^{++})$ hypothesis is further examined using a hypothesis test, in which the alternative hypothesis is our baseline model with an additional $f_J(2480)(J^{PC} = 2^{++}$ or $4^{++})$ state. The changes of NLL when the $f_0(2480)$ is removed from the alternative hypothesis are 25.4 and 30.0, respectively. The significances of the 0^{++} hypothesis over the alternative $J^{PC} = 2^{++}, 4^{++}$ possibilities are then determined to be 6.3σ and 7.0σ.

V. SYSTEMATIC UNCERTAINTIES

The sources of systematic uncertainty are divided into two categories. The first includes the systematic uncertainties from the number of J/ψ events (0.4% [39]), MDC tracking (1.0% each for four charged tracks [40]), pion PID (1.0% each for four pions [41]), photon detection efficiency (1.0% each [42] for five, four photons in mode I and mode II), kinematic fit [43] (1.9%, 0.8% for mode I and mode II), η' mass resolution (0.1%, 0.4% for mode I and mode II), and $\mathcal{B}_{\eta'\to\eta\pi^+\pi^-}$ (0.5% for each $\eta'(\eta\pi^+\pi^-)$), $\mathcal{B}_{\eta'\to\gamma\pi^+\pi^-}$ (0.4% for each $\eta'(\gamma\pi^+\pi^-)$), $\mathcal{B}_{\eta\to\gamma\gamma}$ (0.2% for each η) [13]. These systematic uncertainties are applied separately to the branching fractions for mode I and mode II, and summarized in Table IV. The measurements from these two modes are combined by considering the difference of uncertainties for these two modes. The combination of common and independent systematic uncertainties from the first category is calculated using the weighted least squares method [44]. The combined systematic uncertainty from the first category is 7.0%. The second source comes from the PWA fit procedure, where the systematic uncertainties are applied to measurements of the branching fractions and resonance parameters. These sources of systematic uncertainties are described as below.

TABLE IV. Summary of the first part of the systematic uncertainties for mode I and mode II. The items with * are common uncertainties for these two decay modes.

Source	Mode I	Mode II
MDC tracking*	4.0	4.0
PID*	4.0	4.0
Photon detection*	5.0	4.0
Kinematic fit	1.9	0.8
η' resolution	0.1	0.4
$\mathcal{B}(\eta' \to \eta\pi^+\pi^-)$*	1.0	0.5
$\mathcal{B}(\eta' \to \gamma\pi^+\pi^-)$	…	0.4
$\mathcal{B}(\eta \to \gamma\gamma)$*	0.4	0.2
Number of J/ψ events*	0.4	0.4
Total	7.9	7.0

(i) BW parametrization. The uncertainty from the BW parametrization is estimated by the changes in the fit results caused by replacing the constant width Γ_0 of the BW for $f_0(2020)$, which is close to the $\eta'\eta'$ threshold, with the mass-dependent width as explained in Sec. IV B.

(ii) Background uncertainty. To estimate the background uncertainty, alternative fits are performed with background events from different η' sideband regions and different normalization factors, and the differences of the results are assigned as the systematic uncertainty.

(iii) Uncertainties from additional resonances. Uncertainties from possible additional resonances are estimated by adding the $\rho(1900)$ and the $h_1(1170)$, which are the two most significant additional resonances, into the baseline configuration individually. The changes of the results caused by them are assigned as the systematic uncertainties.

TABLE V. Summary of the systematic uncertainties on the masses (MeV/c^2) and widths (MeV) of the resonances in the baseline model, denoted as ΔM and ΔΓ.

	$f_0(2020)$		$f_0(2330)$		$f_0(2480)$		$h_1(1415)$		$f_2(2340)$	
Sources	ΔM	ΔΓ	ΔM	ΔΓ	ΔM	ΔΓ	ΔM	ΔΓ	ΔM	ΔΓ
Breit-Wigner formula	+45	+26	+2	+29	−6	+11	+1	+3	−1	−4
Extra resonances	+30	$^{+35}_{-49}$	+8	−9	+4	−8	+8	−10	$^{+22}_{-6}$	$^{+26}_{-6}$
Background uncertainty	+2	+14	+5	+7	+1	+3	+4	+12	+1	−10
Total	+54	$^{+46}_{-49}$	+10	$^{+30}_{-9}$	$^{+4}_{-6}$	$^{+11}_{-8}$	+9	$^{+12}_{-10}$	$^{+22}_{-6}$	$^{+26}_{-12}$

TABLE VI. Summary of systematic uncertainties on the branching fraction of $J/\psi \to \gamma X, X \to \eta'\eta'$ or $J/\psi \to \eta' X, X \to \gamma\eta'$ (%).

Sources	$f_0(2020)$	$f_0(2330)$	$f_0(2480)$	$h_1(1415)$	$f_2(2340)$	0^{++} PHSP
First category			±7.0			
Breit-Wigner formula	+6.7	+63.4	+40.7	−5.2	−2.9	+38.0
Extra resonances	−16.3	−26.8	−26.4	−37.9	$^{+0.8}_{-17.5}$	$^{+347.8}_{-59.1}$
Background uncertainty	+6.8	+15.4	+19.4	+14.0	−2.9	+3.0
Total	$^{+11.8}_{-17.7}$	$^{+65.7}_{-27.7}$	$^{+45.6}_{-27.3}$	$^{+15.7}_{-38.9}$	$^{+7.1}_{-19.3}$	$^{+350.0}_{-59.5}$

For each alternative fit performed to estimate the systematic uncertainties from the PWA fit procedure, the changes of the results are taken as the one-sided systematic uncertainties. For each measurement, the individual uncertainties are assumed to be independent and are added in quadrature to obtain the total systematic uncertainty on the negative and positive side, respectively. The sources of systematic uncertainties are applied to the measurements of masses and widths of all resonances, and their contributions are summarized in Table V. The relative systematic uncertainties relevant to the branching fraction measurements are summarized in Table VI, where the last row lists the total relative systematic uncertainties from fitting irrelevant sources.

VI. SUMMARY

In summary, a PWA of the decay $J/\psi \to \gamma\eta'\eta'$ has been performed based on 10.09×10^9 J/ψ events collected with the BESIII detector. The dominant contributions are from the scalars, $f_0(2020)$ and $f_0(2330)$, together with a non-negligible contribution from $f_2(2340)$. The $h_1(1415)$ in $\gamma\eta'$ is also observed. Their measured masses and widths are consistent with the PDG values [13]. A possible new 0^{++} state, $f_0(2480)$, with a significance of 5.2σ, whose mass and width are respectively $2470 \pm 4^{+4}_{-6}$ MeV/c^2 and $75 \pm 9^{+11}_{-8}$ MeV, is needed to describe the data.

The $f_0(2020)$, $f_0(2330)$, and $f_2(2340)$ are observed in the $\eta'\eta'$ decay mode for the first time. The production of $f_0(2020)$ in $J/\psi \to \gamma\eta'\eta'$ is compatible with that of $f_0(2100)$ in $J/\psi \to \gamma\eta\eta$ [11] and $f_0(2200)$ in $J/\psi \to \gamma K^0_S K^0_S$ [12]. If those scalars are assigned to one resonance in this analysis, its large production rate in radiative J/ψ decay suggests that it has a large overlap with scalar glueball. However, its mass is lower than the mass of the first excitation of scalar glueball from the LQCD prediction [6–10]. With the high statistics J/ψ data sample collected with BESIII, it is now critical to study the pole structure of the scalars around 2.1 GeV/c^2 with coupled channel analyses [4,5].

ACKNOWLEDGMENTS

The BESIII Collaboration thanks the staff of BEPCII and the IHEP computing center for their strong support. This work is supported in part by National Key Basic Research Program of China under Contracts No. 2020YFA0406300, No. 2020YFA0406400; National Natural Science Foundation of China (NSFC) under Contracts No. 11625523, No. 11635010, No. 11675183, No. 11735014, No. 11822506, No. 11835012, No. 11922511, No. 11935015, No. 11935016, No. 11935018, No. 11961141012, No. 12022510, No. 12025502, No. 12035009, No. 12035013, No. 12061131003; the Chinese Academy of Sciences (CAS) Large-Scale Scientific Facility Program; Joint Large-Scale Scientific Facility Funds of the NSFC and CAS under Contracts No. U1732103, No. U1732263, No. U1832207; CAS Key Research Program of Frontier Sciences under Contracts No. QYZDJ-SSW-SLH003, No. QYZDJ-SSW-SLH040; 100 Talents Program of CAS; INPAC and Shanghai Key Laboratory for Particle Physics and Cosmology; ERC under Contract No. 758462; European Union Horizon 2020 research and innovation programme under Contract No. Marie Sklodowska-Curie Grant Agreement No. 894790; German Research

Foundation DFG under Contracts No. 443159800, Collaborative Research Center No. CRC 1044, No. FOR 2359, No. FOR 2359, No. GRK 214; Istituto Nazionale di Fisica Nucleare, Italy; Ministry of Development of Turkey under Contract No. DPT2006K-120470; National Science and Technology fund; Olle Engkvist Foundation under Contract No. 200-0605; STFC (United Kingdom); The Knut and Alice Wallenberg Foundation (Sweden) under Contract No. 2016.0157; The Royal Society, UK under Contracts No. DH140054, No. DH160214; The Swedish Research Council; U.S. Department of Energy under Contracts No. DE-FG02-05ER41374, No. DE-SC-0012069.

[1] C. Amsler and N. A. Tornqvist, Phys. Rep. **389**, 61 (2004).
[2] E. Klempt and A. Zaitsev, Phys. Rep. **454**, 1 (2007).
[3] V. Crede and C. A. Meyer, Prog. Part. Nucl. Phys. **63**, 74 (2009).
[4] A. V. Sarantsev, I. Denisenko, U. Thoma, and E. Klempt, Phys. Lett. B **816**, 136227 (2021).
[5] A. Rodas, A. Pilloni, M. Albaladejo, C. Fernandez-Ramirez, V. Mathieu, and A. P. Szczepaniak (JPAC Collaboration), Eur. Phys. J. C **82**, 80 (2022).
[6] G. S. Bali, K. Schilling, A. Hulsebos, A. C. Irving, C. Michael, and P. W. Stephenson (UKQCD Collaboration), Phys. Lett. B **309**, 378 (1993).
[7] C. J. Morningstar and M. J. Peardon, Phys. Rev. D **60**, 034509 (1999).
[8] Y. Chen, A. Alexandru, S. J. Dong, T. Draper, I. Horváth, F. X. Lee, K. F. Liu, N. Mathur, C. Morningstar, M. Peardon, S. Tamhankar, B. L. Young, and J. B. Zhang, Phys. Rev. D **73**, 014516 (2006).
[9] E. Gregory, A. Irving, B. Lucini, C. McNeile, A. Rago, C. Richards, and E. Rinaldi, J. High Energy Phys. 10 (2012) 170.
[10] W. Sun, L.-C. Gui, Y. Chen, M. Gong, C. Liu, Y.-B. Liu, Z. Liu, J.-P. Ma, and J.-B. Zhang, Chin. Phys. C **42**, 093103 (2018).
[11] M. Ablikim *et al.* (BESIII Collaboration), Phys. Rev. D **87**, 092009 (2013).
[12] M. Ablikim *et al.* (BESIII Collaboration), Phys. Rev. D **98**, 072003 (2018).
[13] P. A. Zyla *et al.* (Particle Data Group), Prog. Theor. Exp. Phys. **2020**, 083C01 (2020).
[14] L.-C. Gui, Y. Chen, G. Li, C. Liu, Y.-B. Liu, J.-P. Ma, Y.-B. Yang, and J.-B. Zhang (CLQCD Collaboration), Phys. Rev. Lett. **110**, 021601 (2013).
[15] A. V. Anisovich, C. A. Baker, C. J. Batty, D. V. Bugg, C. Hodd, H. C. Lu, V. A. Nikonov, A. V. Sarantsev, V. V. Sarantsev, and B. S. Zou, Phys. Lett. B **491**, 47 (2000).
[16] A. V. Anisovich, C. A. Baker, C. J. Batty, D. V. Bugg, A. Hasan, C. Hodd, J. Kisiel, V. A. Nikonov, A. V. Sarantsev, V. V. Sarantsev, and B. S. Zou, Nucl. Phys. **A662**, 319 (2000).
[17] A. Etkin, K. J. Foley, R. W. Hackenburg, R. S. Longacre, W. A. Love, T. W. Morris, E. D. Platner, A. C. Saulys, S. J. Lindenbaum, C. Chan, and M. A. Kramer, Phys. Lett. B **201**, 568 (1988).
[18] M. Ablikim *et al.* (BESIII Collaboration), Phys. Rev. D **93**, 112011 (2016).
[19] M. Ablikim *et al.* (BESIII Collaboration), Phys. Rev. D **92**, 052003 (2015).
[20] Y.-B. Yang, L.-C. Gui, Y. Chen, C. Liu, Y.-B. Liu, J.-P. Ma, and J.-B. Zhang (CLQCD Collaboration), Phys. Rev. Lett. **111**, 091601 (2013).
[21] M. Ablikim *et al.* (BESIII Collaboration), arXiv:2111.07571.
[22] M. Ablikim *et al.* (BESIII Collaboration), Nucl. Instrum. Methods Phys. Res., Sect. A **614**, 345 (2010).
[23] M. Ablikim *et al.* (BESIII Collaboration), Chin. Phys. C **44**, 040001 (2020).
[24] X. Li, Y. Sun, C. Li, Z. Liu, Y. Heng, M. Shao, X. Wang, Z. Wu, P. Cao, and M. Chen, Radiat. Detect. Technol. Methods **1**, 13 (2017); Y. X. Guo, S. S. Sun, F. F. An, R. X. Yang, M. Zhou, Z. Wu, H. L. Dai, Y. K. Heng, C. Li, and Z. Y. Deng, Radiat. Detect. Technol. Methods **1**, 15 (2017); P. Cao *et al.*, Nucl. Instrum. Methods Phys. Res., Sect. A **953**, 163053 (2020).
[25] S. Agostinelli *et al.* (GEANT4 Collaboration), Nucl. Instrum. Methods Phys. Res., Sect. A **506**, 250 (2003).
[26] S. Jadach, B. F. L. Ward, and Z. Was, Phys. Rev. D **63**, 113009 (2001); Comput. Phys. Commun. **130**, 260 (2000).
[27] D. J. Lange, Nucl. Instrum. Methods Phys. Res., Sect. A **462**, 152 (2001); R.-G. Ping, Chin. Phys. C **32**, 599 (2008).
[28] J. C. Chen, G. S. Huang, X. R. Qi, D. H. Zhang, and Y. S. Zhu, Phys. Rev. D **62**, 034003 (2000); R.-L. Yang, R.-G. Ping, and H. Chen, Chin. Phys. Lett. **31**, 061301 (2014).
[29] E. Richter-Was, Phys. Lett. B **303**, 163 (1993).
[30] M. Ablikim *et al.* (BESIII Collaboration), Phys. Rev. Lett. **120**, 242003 (2018).
[31] M. Ablikim *et al.* (BESIII Collaboration), Chin. Phys. C **45**, 023002 (2021).
[32] N. Berger, K. Zhu, Z.-A. Liu, D.-P. Jin, H. Xu, W.-X. Gong, K. Wang, and G.-F. Cao, Chin. Phys. C **34**, 1779 (2010).
[33] X. Zhou, S. Du, G. Li, and C. Shen, Comput. Phys. Commun. **258**, 107540 (2021).
[34] N. Berger, B. Liu, and J. Wang, J. Phys. Conf. Ser. **219**, 042031 (2010).
[35] B. S. Zou and D. V. Bugg, Eur. Phys. J. A **16**, 537 (2003).
[36] F. James and M. Roos, Comput. Phys. Commun. **10**, 343 (1975).
[37] D. V. Bugg, Phys. Rep. **397**, 257 (2004).
[38] E. Gross and O. Vitells, Eur. Phys. J. C **70**, 525 (2010).
[39] M. Ablikim *et al.* (BESIII Collaboration), Chin. Phys. C **41**, 013001 (2017).
[40] M. Ablikim *et al.* (BESIII Collaboration), Phys. Rev. D **85**, 092012 (2012).

[41] M. Ablikim *et al.* (BESIII Collaboration), Phys. Rev. D **83**, 112005 (2011).
[42] M. Ablikim *et al.* (BESIII Collaboration), Phys. Rev. D **81**, 052005 (2010).
[43] M. Ablikim *et al.* (BESIII Collaboration), Phys. Rev. D **87**, 012002 (2013).
[44] G. D'Agostini, Nucl. Instrum. Methods Phys. Res., Sect. A **346**, 306 (1994).